

Structural, spectral, electrical, Z-scan and HOMO LUMO studies on new 2-amino-6-methylpyridinium 2-hydroxybenzoate crystal

B. PUNITHAVENI^{1,*}, K. THILAGAVATHY², N. MUTHUKUMARASAMY², D. NITHYAPRAKASH³,
M. SARAVANABHAVAN⁴

¹Department of Physics, Tamilnadu College of Engineering, Coimbatore-641 659, Tamilnadu, India

²Department of Physics, Coimbatore Institute of Technology, Coimbatore-641 014, Tamilnadu, India

³Department of Physics, PPG Institute of Technology, Coimbatore-641 035, Tamilnadu, India

⁴Department of Chemistry, Dr. N.G.P. Institute of Technology, Coimbatore-641048, Tamilnadu, India

New organic single crystals of 2-amino-6-methylpyridinium 2-hydroxybenzoate (2A6M2H) were grown by slow evaporation solution growth technique at room temperature. The grown crystal structure was studied using single crystal XRD. Crystalline nature and phases were confirmed by powder XRD analysis. FT-IR study was used to identify the functional groups present in the compound. UV-Vis study revealed that the lower cut off wavelength of the crystal is at 350 nm. The dielectric studies indicated the low value of dielectric loss at high frequency. Mechanical properties of the crystals were studied using Vickers microhardness test. The Z-Scan studies were conducted for the crystal using He-Ne laser.

Keywords: *slow evaporation; non-linear optics; dielectric studies*

1. Introduction

After invention of laser in 1940 there has been a steady development in the frequency doubling process, nearly for the last five decades. Materials with high NLO characteristics are of great interest in view of their vital applications, such as second and third harmonic generation, electro-optical amplitude modulation, high density optical data storage, ultra-compact lasers, optical switching, optical limiting, optical logics, THz wave generation, frequency shifting, optical parametric generation, medical diagnosis and bio photonics [1–3]. In this regard, a great number of inorganic, organic and semi organic crystals have already been grown and their NLO properties reported. But still the quest for more efficient nonlinear optical materials is on the increase for the future development of the optoelectronics and photonics technology. Organic materials are considered to be promising NLO candidates since they have several advantages,

such as high crystalline nature, flexibility of molecular design, high laser damage threshold and large second order hyperpolarizability β , when compared to inorganic counterparts. Particularly charge transfer complexes CT of organic materials are considered for the reason that the special type of interaction is accompanied by the transfer of an electron from the donor to the acceptor. Also this CT complex is based on π - π interaction which leads to high electron density thus providing a fast response to electro-optic effect [4–7]. Pyridinium derivatives have optical, pharmaceutical and biological applications and also they easily form hydrogen bonding with carboxylic acids [8–10]. Previously, many pyridine-acid derivatives were synthesized and their properties were analyzed. Salicylic acid is one of the organic biomolecules subjected to demanding research as it possesses a great potential for a wide range of applications in medicine, agriculture and photosynthesis [11].

Based on these facts, pyridine-acid based (donor-acceptor) crystal: 2-amino-6-methylpyridinium was grown and the third order

*E-mail: punithip12@gmail.com

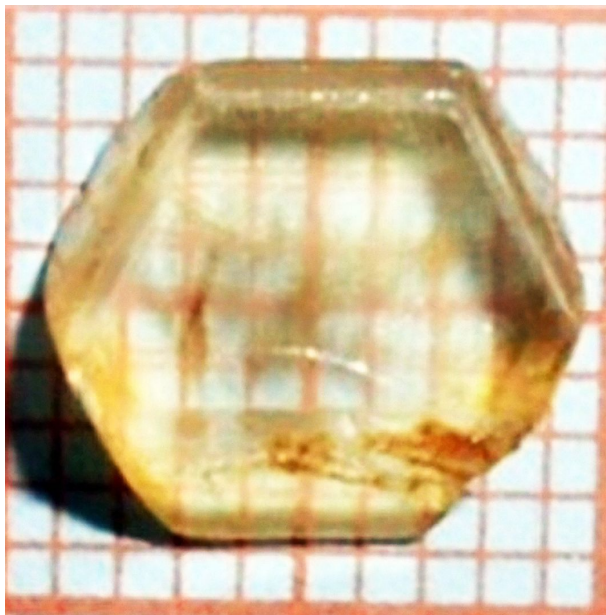


Fig. 1. As-grown crystal of 2A6M2H.

nonlinear optical parameters, such as nonlinear refractive index and nonlinear absorption coefficient have been calculated and discussed in detail.

2. Experimental

2.1. Crystal growth

In the present work, 2A6M2H crystals were grown by slow evaporation solution growth technique at room temperature. Commercially accessible 2-amino-6-methylpyridine ($C_6H_8N_2$) (Aldrich) and 2-hydroxybenzoic acid ($C_7H_6O_3$) (Hi-media) were taken in the molar ratio of 1:1 and dissolved in methanol, and the solution was thoroughly stirred for 2 h using a magnetic stirrer to yield a homogeneous mixture solution. Then the homogeneous solution was filtered using Whatman filter paper (No. 42) and transferred into a crystallizing vessel. In order to control the evaporation rate, the top of the beaker was covered with a thin plastic sheet and the content was subjected to a slow evaporation process at room temperature. After six days, crystals were harvested from the mother solution. The grown crystal is shown in Fig. 1.

2.2. Characterization techniques

2.2.1. Spectroscopic studies

Single crystal X-ray diffraction (SXRD) is an analytical technique to determine the arrangement of atoms in a crystal. The unit cell parameters and the crystal structure of the synthesized compound were obtained on a Bruker AXS Kappa APEX IICCD diffractometer using graphite monochromated $MoK\alpha$ radiation ($\lambda = 0.71073 \text{ \AA}$) at 273 K. The structure was solved by a direct method using the SHELXS 97 [12] program and refined with SHELXL 97 by full matrix least-square procedure. The molecule graphics were prepared using the ORTEP [13]. The final refinement converged to R-values of $R1 = 0.045$ and $wR2 = 0.125$. The grown crystals of 2A6M2H were subjected to UV-Vis-NIR spectral analysis using Perkin Elmer Lambda 35 spectrometer with the wavelength range of 200 nm to 1100 nm, to study linear optical characteristics of the sample. The presence of characteristic absorption bands in the grown 2A6M2H were recorded at room temperature in the range of 400 cm^{-1} to 4000 cm^{-1} using a Bruker FT-IR 4100 spectrometer. Dielectric studies were carried out by using Hioki 3532-50 LCR meter. Mechanical studies of the 2A6M2H crystals were carried out at room temperature by using a Leitz-Wetzlar microhardness tester fitted with a Vickers diamond pyramidal indenter attached to an incident light microscope. A He-Ne laser with a fundamental wavelength of 632.8 nm, a repetition rate of 1 kHz and a pulse width of 8 ns was used as an optical source for third nonlinear optical susceptibility measurements.

2.2.2. Quantum chemical studies

The theoretical quantum chemical studies were performed by DFT (B3LYP Becke three-parameter B3 exchange in conjunction with the Lee-Yang-Parr LYP correlation functional) method with B3LYP/6-31G basis set using Gaussian 09 program [14]. Gauss View 5.0 visualization program [15] has been employed to shape HOMO, LUMO orbitals.

3. Results and discussion

3.1. X-ray diffraction analysis

The single crystal XRD studies clearly show that the grown crystals of 2A6M2H belong to tetragonal crystal system (space group $I4_1/a$) with unit cell parameters $a = 14.1410 (50) \text{ \AA}$, $b = 14.1410 (50) \text{ \AA}$, $c = 24.6890 (50) \text{ \AA}$, $\alpha = 90^\circ$, $\beta = 90^\circ$, $\gamma = 90^\circ$. The unit cell volume is 4937.01 \AA^3 . The number of molecules per unit cell Z is eight. The crystal data and collected parameters are given in Table 1. The molecular graphics have been prepared by using the results obtained by DFT [13]. The ORTEP representation of the compound is shown in Fig. 2. The crystal data confirm that the protonation occurs in the 2-amino-6-methyl-pyridinium-2-hydroxy-benzoate molecules. The hydrogen from the carboxylic acid group in 2-hydroxybenzoic acid is transferred to the nitrogen atom in the pyridine ring. Fig. 3 shows the crystal packing diagram along the c axis. The hydrogen bonds in the crystal stabilize the crystal structure.

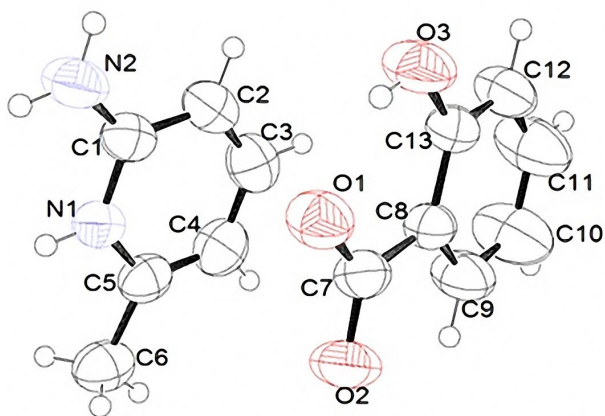


Fig. 2. ORTEP diagram of 2A6M2H.

Powder X-ray diffraction patterns of the grown crystals were obtained by using a Rich Seifert diffractometer. Diffraction pattern data were collected on the diffractometer equipped with monochromated $\text{CuK}\alpha$ radiation (1.540598 \AA) and detected by a scintillation counter. The grown crystals were finely crushed into powder and subjected to analysis. The sample was scanned over

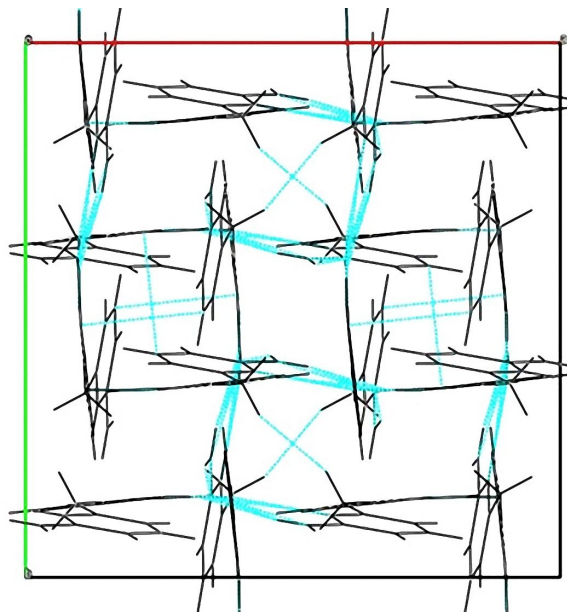


Fig. 3. Packing diagram of 2A6M2H.

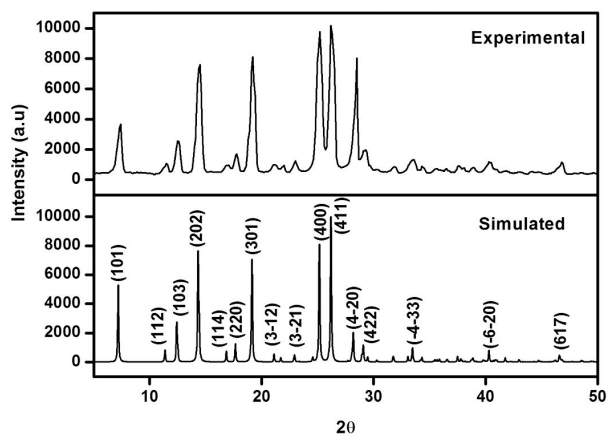


Fig. 4. Comparison of experimental and simulated powder XRD patterns of 2A6M2H.

a 2θ range of 5° to 60° at a scan rate of $1/\text{min}$. Fig. 4 depicts the powder X-ray pattern for the 2A6M2H crystal. The sharp and well defined Bragg peaks at specific 2θ angle confirm the crystalline nature of the sample. The experimental XRD pattern was compared with the simulated one, generated from crystallographic information file (CIF) and both are in good agreement with each other.

Table 1. Crystal data and structure refinement for 2A6M2H.

Empirical formula	C ₂₆ H ₂₈ N ₄ O ₆
Formula weight	492.5
Temperature	273(2) K
Wavelength	0.71073 Å
Crystal system, space group	Tetragonal I4 ₁ /a
Unit cell dimensions	a = 14.1410 (50) Å b = 14.1410(50)(5) Å c = 24.6890 (50)(4) Å
Volume	4937.01 Å ³
Z, Calculated density	8, 1.33 M·gm ⁻³
Limiting indices	-16 ≤ h ≤ 18 -16 ≤ k ≤ 18 -31 ≤ l ≤ 32
Final R indices [I > 2σ(I)]	R1 = 0.045 wR2 = 0.125
R indices (all data)	R1 = 0.085 wR2 = 0.147
CCDC No.	1501662

3.2. FT-IR analysis

The presence of characteristic absorption bands in the grown single crystal has been studied by FT-IR analysis. The FT-IR spectrum of 2A6M2H crystal is shown in the Fig. 5. The band at 3665 cm⁻¹ is due to the O–H stretching vibration. The peak at 3288 cm⁻¹ is attributed to NH stretching frequency in the protonated nitrogen of the pyridinium moiety. The amine NH₂ stretching vibration is observed at 3023 cm⁻¹. The broad peaks at 2800 cm⁻¹ and 2703 cm⁻¹ are also assigned to the H–C=O vibration. The CH stretching vibration is observed at 2617 cm⁻¹. The absorptions at 1923 cm⁻¹ and 1685 cm⁻¹ are due to C=O and C–C stretching vibrations. The NH bending vibration is observed at 1640 cm⁻¹. The COO⁻ stretching vibration is observed at 1578 cm⁻¹ and 1456 cm⁻¹. The CH rocking vibration is attributed to the peak at 1386 cm⁻¹. The C=C stretching vibration is observed at 1345 cm⁻¹. The absorptions at 1302 cm⁻¹ and 1247 cm⁻¹

are due to CN stretching vibrations. The OH in-plane and out-plane bending vibrations are observed at 1172 cm⁻¹ and 949 cm⁻¹, respectively. The absorption at 1142 cm⁻¹ is due to C–O stretching vibration. The absorptions at 1031 cm⁻¹ and 992 cm⁻¹ are due to CH in- and out-plane bending vibrations respectively. The sharp absorption band at 842 cm⁻¹ is attributed to NH out-plane bending vibration. The absorption at 783 cm⁻¹ is due to NH wagging vibration. The absorption band at 742 cm⁻¹ is attributed to COO⁻ scissoring vibration. The OH out-plane bending vibration is observed at 663 cm⁻¹. Hence, the functional groups are present in the title compound.

3.3. Optical studies

The grown crystals of 2A6M2H were subjected to UV-Vis-NIR spectral analysis in the wavelength range from 200 nm to 1100 nm, to study linear optical characteristics of the sample. The electronic absorption spectrum of 2A6M2H was compared

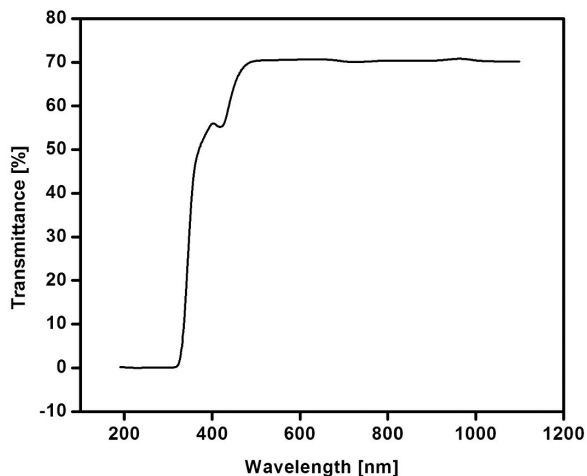


Fig. 5. FT-IR spectrum of 2A6M2H.

with the parent compounds and is depicted in Fig. 6. For pure 2-amino 6-methylpyridine, two absorption bands are observed at 235 nm and 300 nm ($\pi \rightarrow \pi^*$ and $n \rightarrow \pi^*$). Also for 2-hydroxybenzoic acid, the bands are noted at 210 nm, 229 nm and 300 nm. Fascinatingly, the mixed compound exhibits two absorptions: one is around 238 nm ($\pi \rightarrow \pi^*$) which merely coincides with the pure pyridine and the acid wavelengths. However, a new peak at 269 nm ($n \rightarrow \pi^*$) confirms the charge transfer between the donor and acceptor. The transmittance spectrum is depicted in Fig. 7. The improved optical transmittance is one of the most important properties in the NLO crystalline compounds. From the spectrum, it is clear that UV cut-off wavelength of the grown 2A6M2H crystal is noted around 350 nm. The crystal is entirely transparent beyond the cut-off wavelength up to 1100 nm. The band structure and type of transition of electrons was studied by means of the dependence of optical absorption coefficient on the photon energy [16].

The optical absorption coefficient α of the grown crystal was obtained from the following relation:

$$\alpha = \frac{2.303 \log (1/T)}{d} \quad (1)$$

where d is the thickness of the crystal and T is the transmittance.

The absorption coefficient α of 2A6M2H was determined using the following relation:

$$(\alpha h\nu) = A(h\nu - E_g)^n \quad (2)$$

where A is a constant, h is the Planck constant and ν is frequency of incident photons. The above equation is well suitable for allowable direct transition between simple parabolic bands. The optical energy gap E_g of 2A6M2H calculated using the plot of $(\alpha h\nu)^{1/n}$ versus $h\nu$, by extrapolating the linear portion of the curve [17] is shown in Fig. 8. The band gap value of 2A6M2H crystal is estimated at 3.358 eV. The wide band gap of this crystal suggests large transmittance of visible region.

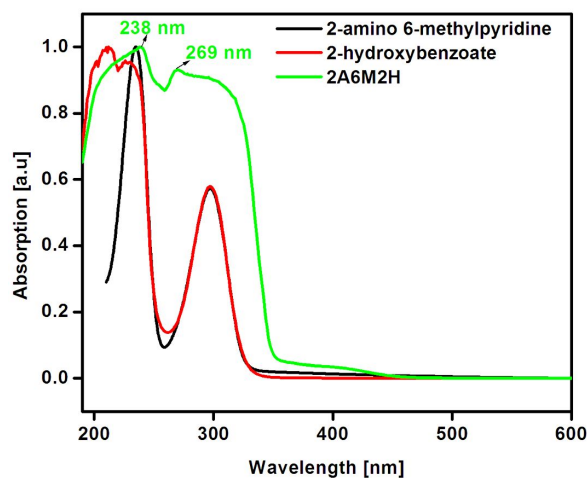


Fig. 6. Absorption spectrum of 2A6M2H.

3.4. Dielectric studies

The grown crystal was subjected to dielectric measurement. Two opposite surfaces across the width of the sample were coated with a good quality silver paste in order to obtain good ohmic contact. The capacitance of the crystal was measured in the frequency range of 50 Hz to 200 kHz at various temperatures. Fig. 9 shows the plot of dielectric constant ϵ_r versus frequency at temperatures of 303 K, 313 K, 323 K and 333 K. The dielectric constant of the crystal was calculated using the relation $\epsilon_r = C_{\text{cryst}}d/\epsilon_0A$, where C_{cryst} is the capacitance of the crystal, d is the thickness, ϵ_0 is free space permittivity and A is the area of the sample. The dielectric constant has higher values

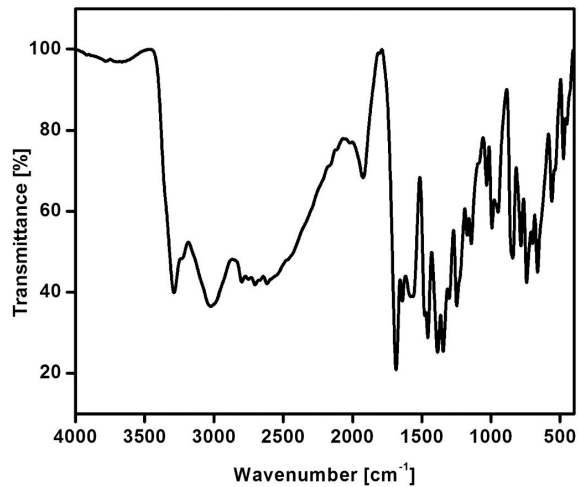


Fig. 7. Transmittance spectrum of 2A6M2H.

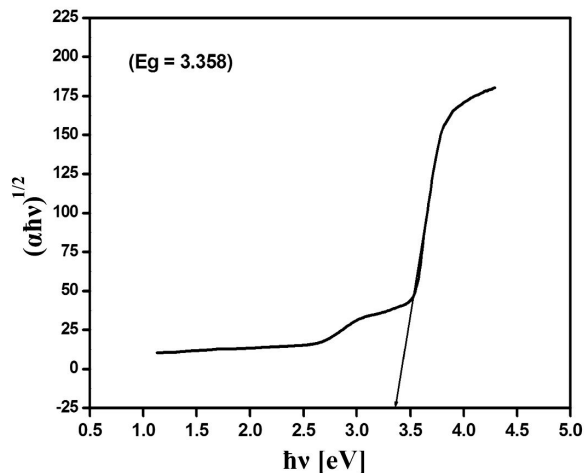


Fig. 8. Optical bandgap of 2A6M2H.

in the low frequency region and then it decreases with increasing frequency. The dielectric constant increases also with the raise of temperature. The very high values of dielectric constant at low frequencies may be due to the presence of space charge, orientation, electronic and ionic polarizations. In these polarizations, space charge polarization depends on the perfection and purity of the sample. Thus, in the present system space charge polarization is active at the low frequency region and high temperature [18, 19]. The variation of dielectric loss with log frequency is shown in Fig. 10. The dielectric loss is very low at a high frequency.

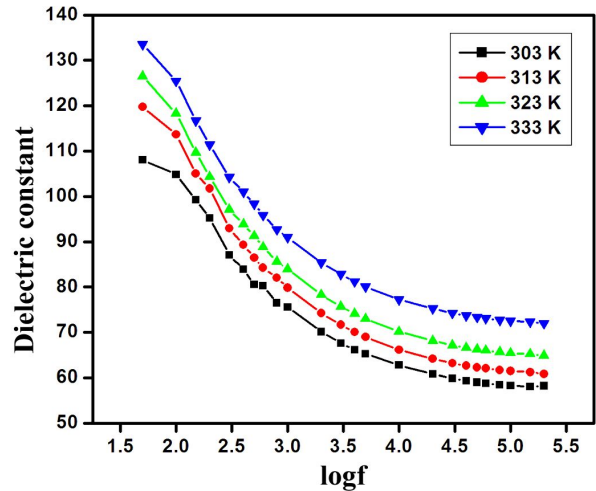


Fig. 9. Dielectric constant vs. logf.

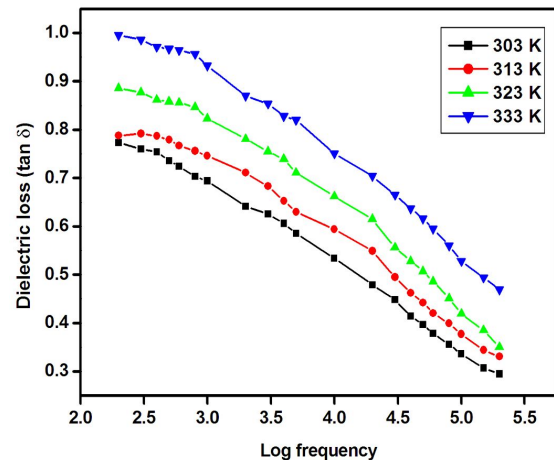


Fig. 10. Dielectric loss vs. logf.

Materials with a high dielectric constant are characterized by higher power dissipation [20].

Since the dielectric constant and loss values of 2A6M2H crystals were found to be low, the crystals are suitable for electro-optical applications [21, 22].

3.5. Hardness studies

Hardness is the resistance offered by a material to localized plastic deformation caused by scratching or indentation. The indentation hardness is measured as a ratio of applied load to the surface of the indentation. Microhardness studies

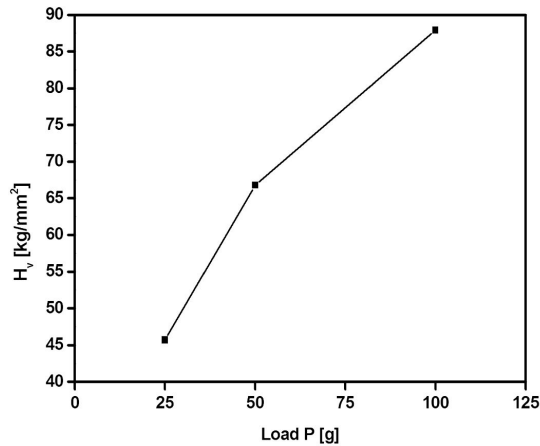


Fig. 11. Hardness vs. applied load.

were carried out on 2A6M2H crystal using a Leitz-Wetzlar microhardness tester fitted with a Vickers diamond pyramidal indenter attached to an incident light microscope. The static indentations were made at room temperature with a constant indentation time of 10 s for all indentations. The indentation marks were made on the surfaces by varying the load from 25 g to 100 g. As microcracks developed at higher loads, the maximum applied load was restricted to 100 g only. The Vickers microhardness number HV of the crystal was calculated using the relation $HV = 1.8544 P/d^2$ Pa, where P is the applied load and d is the average diagonal length of the indented impressions in meter. Vickers microhardness profile as a function of the applied test load is illustrated in Fig. 11. It is evident from the plot that the change in microhardness values of 2A6M2H with increasing load is in good agreement with the normal indentation size effect (ISE). The value of the work hardening coefficient n was estimated from the plot (Fig. 12) of $\log P$ versus $\log d$ drawn using the least square fit method. It is observed that the Vickers hardness number and the work hardening coefficients of the crystal decrease with increasing load. According to Onitsch [23], the relation: $1.0 \leq n \leq 1.6$ is valid for hard materials and $n > 1.6$ is applicable for soft materials.

The calculated n value is found to be greater than 1.6. Hence, 2A6M2H crystal belongs to soft material category.

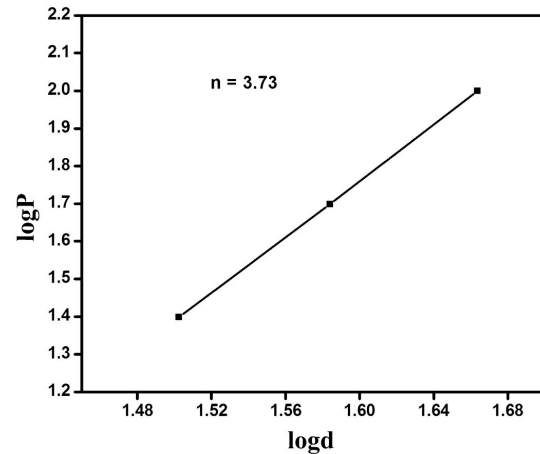


Fig. 12. XRD of CuO NWs on Ti-coated glass substrates oxidized at 400 °C (a), and at 500 °C (b) for 4 h in the air.

3.6. Z-scan studies

The Z-scan is a well-known experimental technique used to measure the third order nonlinear susceptibility of the materials [24, 25]. The nonlinear optical parameters were measured by using single beam Z-scan technique with He-Ne laser source. The sample was moved across a focal region ($-Z$ to $+Z$) along the axial direction, which was the direction of propagation of the laser beam. The Gaussian beam was focused by a convex lens to produce the beam waist of 12.22 μm and the focal spot size was measured by using the knife-edge scan method [26]. The open and closed aperture Z-scan configurations were used to investigate the nonlinear absorption coefficient β and nonlinear refractive index n_2 , respectively. Fig. 13 shows the normalized transmittance T with open aperture as a function of the distance z along the lens axis in the far field and Fig. 14 shows the normalized transmittance T with closed aperture as a function of the distance z along the lens axis in the far field.

The nonlinear refractive index n_2 of the crystal was calculated using the standard relation given below:

$$\Delta\phi_0 = \frac{\Delta T_{p-v}}{0.406 (1-s)^{0.25}} \quad (3)$$

where ΔT_{p-v} is the difference between the normalized peak and valley transmittance and S is the linear transmittance of the aperture.

The nonlinear refractive index n_2 and nonlinear absorption coefficient β are given by:

$$n_2 = \frac{\Delta\phi_0}{kL_{eff}I_0}n_2 = \frac{\Delta\phi}{kI_0L_{eff}} \text{ and } \beta = \frac{2\sqrt{2}\Delta T}{I_0L_{eff}} \quad (4)$$

where k is the wave number $k = 2\pi/\lambda$ and:

$$L_{eff} = \frac{1 - e^{(-\alpha L)}}{\alpha} \quad (5)$$

with $I_0 = \frac{P}{\pi\omega_0^2}$ defined as the peak intensity within the sample, where L is the thickness of the sample, and α is the linear absorption coefficient.

The real and imaginary parts of the third order nonlinear susceptibility χ^3 are defined as:

$$Re\chi^{(3)} = 10^{-4} \frac{(\epsilon_0 C^2 n_0^2 n^2)}{\pi} (esu) \quad (6)$$

$$Im\chi^{(3)} = 10^{-2} \frac{(\epsilon_0 C^2 n_0^2 \lambda \beta)}{4\pi^2} (esu) \quad (7)$$

where ϵ_0 is the vacuum permittivity, n_0 is the linear refractive index of the sample and c is the velocity of light in vacuum.

The absolute value of χ^3 is obtained using the following formula:

$$|\chi^{(3)}| = [(Re\chi^{(3)})^2 + (Im\chi^{(3)})^2]^{\frac{1}{2}} \quad (8)$$

As seen from the closed aperture Z scan curve, the pre-focal transmittance valley is followed by the post focal peak which exhibits positive nonlinearity [27].

The calculated values of the nonlinear refractive index n_2 , nonlinear absorption coefficient β and third order susceptibility are given in Table 2 and the obtained results are compared with the other materials and listed in Table 3 [28, 29]. The obtained positive refractive index is ascribed to the thermo-optic process [30].

3.7. HOMO-LUMO analysis

The highest occupied molecular orbitals HOMO and the lowest-lying unoccupied molecular orbitals LUMOs are termed as frontier

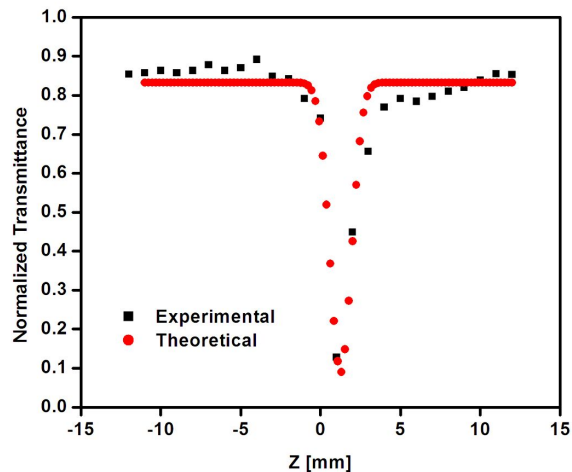


Fig. 13. Normalized transmittance with open aperture as a function of Z position.

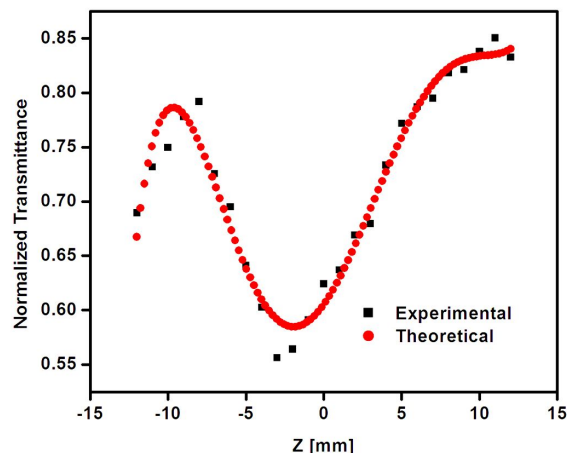


Fig. 14. Normalized transmittance with closed aperture as a function of Z position.

molecular orbitals FMOs. The FMOs play a vital role in the optical and electric properties, as well as in quantum chemistry and UV-Vis spectra [31]. The HOMO exemplifies the ability to donate an electron, LUMO, as an electron acceptor, embodies the ability to acquire an electron. The energy gap between HOMO and LUMO regulates the kinetic stability, chemical reactivity, optical polarizability and chemical hardness-softness of a molecule [32, 33].

The highest occupied MOs (HOMO), the lowest unoccupied MOs (LUMO) were calculated using B3LYP/6-31G.

Table 2. Parameters measured in Z-scan experiment for 2A6M2H.

Laser beam wave length λ	= 632.8 nm
Beam radius of the aperture ω_a	= 1 mm
Aperture radius r_a	= 4 mm
Beam radius ω_o	= 12.22 μm
Incident intensity at the focus $Z = 0$	= 1 MW/cm ²
Effective thickness L_{eff}	= 1.32 mm
Nonlinear refractive index n_2	= 4.68×10^{-8} cm ² /W
Nonlinear absorption coefficient β	= 0.179×10^{-3} cm/W
Real part of the third-order nonlinear susceptibility $\text{Re } \chi^{(3)}$	= 1.47×10^{-7} esu
Imaginary part of the third-order nonlinear susceptibility $\text{Im } \chi^{(3)}$	= 2.84×10^{-9} esu
The third-order nonlinear susceptibility $\chi^{(3)}$	= 1.48×10^{-7} esu

Table 3. Comparative analysis of 2A6M2H crystal and other crystals reported in the literature.

$\chi^{(3)}$	Material	Literature
1.48×10^{-7} esu	2A6M2H	Present work
4.343×10^{-7} esu	Ammonium 3-carboxy-4-hydroxy benzenesulfonate monohydrate	[27]
2.863×10^{-4} esu	γ -glycine	[29]

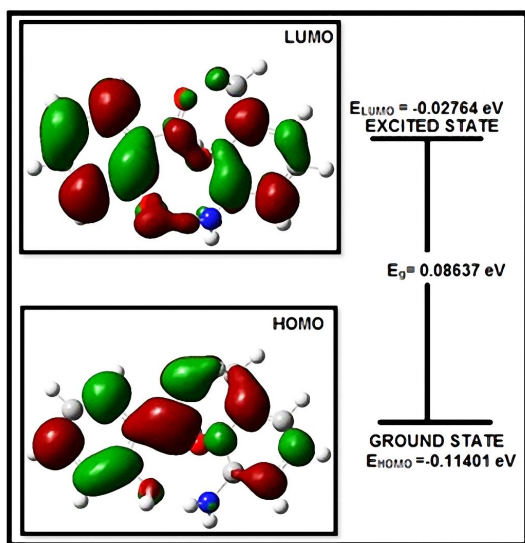


Fig. 15. The molecular orbitals and energies for the HOMO and LUMO of 2A6M2H.

The HOMO and LUMO values are -0.11401 and -0.02764 , respectively. The 3D plots of the HOMO, LUMO orbitals computed at the B3LYP/6-31G level for 2A6M2H molecule are shown in Fig. 15. The positive phase is red

and the negative one is green. It is clear from the figure that, while the HOMO is localized on almost the whole molecule, LUMO is localized on the pyridine benzene ring. Both the HOMO and the LUMO are mostly π anti-bonding type orbitals. The value of energy separation between the HOMO and the LUMO is 0.08637 eV. The energy gap of HOMO-LUMO displays the biological activity of the molecule.

4. Conclusions

Optically good quality 2A6M2H crystals were grown by slow evaporation solution growth technique at room temperature. Single crystal XRD pattern revealed that the 2A6M2H crystal belongs to a tetragonal system with the space group of $I4_1/a$. Functional groups present in the crystals were confirmed by FT-IR technique. Optical transmittance and absorption study exhibited that the crystal is transparent in the entire visible region. Dielectric study showed a low value of dielectric loss at high frequencies. Microhardness studies confirmed the soft nature of the 2A6M2H crystal. Z-scan study revealed the thermo-optic effect

in the crystal. HOMO-LUMO analysis confirmed the charge transfer interaction between the molecules. All the results suggest that the grown 2A6M2H crystal is suitable for optoelectronic applications.

References

- [1] KRISHNAKUMAR V., RAJABOOPATHI M., NAGALAKSHMI R., *Physica B*, 407 (2012), 1119.
- [2] LAXMINARAYANA KAMAT H., MANJUNATHA K.B., SEETHARAM SHETTIGA R., UMESH G., NARAYANA B., SAMSHUDDIN S., SAROJINI B.K., *Opt. Las. Technol.*, 56 (2014), 425.
- [3] SUDHARSAN N., KEETHANA B., NAGALAKSHMI R., KRISHNAKUMAR V., GURUPRASAD L., *Mater. Chem. Phys.*, 134 (2012), 736.
- [4] CHEN T., SUN Z., SONG C., GE Y., LUO J., LIN W., HONG M., *Cryst. Growth Des.*, 12 (2012), 2673.
- [5] BABU A.G., RAMASAMY P.R., RAMASAMY P., *Mater. Chem. Phys.*, 117 (2009), 326.
- [6] SHANMUGAM G., BRAHADEESWARAN S., *Spectrochim. Acta A*, 95 (2012), 177.
- [7] MOOVENDARAN K., SRINIVASAN B.R., KALYANA SUNDAR J., DHAS M.B.S.A., NATARAJAN S., *Spectrochim. Acta A*, 92 (2012), 388.
- [8] THANIGAIMANI K., CHEKHALIB N., ARSHAD S., RAZAK I.A., SIVAJEYANTHI P., *Mol. Cryst. Liquid. Cryst.*, 607 (2015), 156.
- [9] THIRUPUGALMANI K., KARTHICK S., SHANMUGAM G., KANNAN V., SRIDHAR B., NEHRU K., BRAHADEESWARAN S., *Opt. Mater.*, 49 (2015), 158.
- [10] CHANDRA L., CHANDRASEKARAN J., PERUMAL K., BABU B., *Optik*, 127 (2016), 3206.
- [11] MEENATCHI V., MUTHU K., RAJASEKAR M., MEENAKSHI SUNDARAM S.P., MOJUMDAR S.C., *J. Therm. Anal. Calorim.*, 108 (2012), 895.
- [12] SHELDRICK G.M., *SHELXL-97 and SHELXS-97, Structure Determination Software*, University of Göttingen, Germany, 1997.
- [13] FARRUGIA L.J., *J. Appl. Cryst.*, 32 (1999), 837.
- [14] FRISCH M.J. ET AL., 2009, Gaussian 09, Revision C.02. Gaussian, Inc., Wallingford CT.
- [15] DENNINGTON R.I., KEITH T., MILLAM J., EPPINETT K., HOVELL W., 2003, Gauss View Version 3.09.
- [16] TIGAU N., CIUPINA A. V., PRODANA G., RUSUB G.I., GHEORGHIES C., VASILEC E., *J. Optoelectron. Adv. Mater.*, 6 (2004), 211.
- [17] CHAWLA A.K., KAUR D., CHANDRA R., *Opt. Mater.*, 29 (2007), 33.
- [18] BABU B., CHANDRASEKARAN J., BALAPRABHAKARAN S., *Mater. Sci.-Poland*, 32 (2014), 164.
- [19] BABU B., CHANDRASEKARAN J., BALAPRABHAKARAN S., ILAYABARATHI P., *Mater. Sci.-Poland*, 31 (2013), 151.
- [20] ARJUNAN S., BHASKARAN A., MOHAN KUMAR R., MOHAN R., JAYAVEL R., *Mater. Manuf. Process.*, 27 (2012), 49.
- [21] SHANMUGAM G., THIRUPUGALMANI K., RAKHIKRISHNA R., PHILIP J., BRAHADEESWARAN S., *J. Therm. Anal. Calorim.*, 114 (2013), 1245.
- [22] VON HUNDELSHAUSEN U., *Phys. Lett. A*, 34 (1971), 405.
- [23] ONITSCH E.M., *Mikroskopie*, 2 (1947), 131.
- [24] SHEIK-BAHAIE M., SAID A.A., VAN STRYLAND E.W., *Opt. Lett.*, 14 (1989), 955.
- [25] PAPAGIANNOULI I., ILIOPOULOS K., GINDRE D., SAHRAOUI B., KRUPKA O., SMOKAL V., KOLENDO A., COURIS S., *Chem. Phys. Lett.*, 554 (2012), 107.
- [26] VESHAPIDZE G., TRACHY M.L., SHAH M.H., DE-PAOLA B.D., *Appl. Opt.*, 32 (2006), 8197.
- [27] GOMEZ S.L., CUPPO F.L.S., FIGUERIREDO NETO A.M., *Br. J. Phys.*, 33 (2003), 813.
- [28] SHEIK-BAHAIE M., SAID A., WEI T.H., HAGAN D.J., STRYLAND VAN E.W., *IEEE J. Quantum Electron.*, 27 (1990), 760.
- [29] SILAMBARASAN A., KRISHNA KUMAR M., THIRUNAVUKKARASU A., MOHAN KUMAR R., UMARAN P.R., *Spectrochim. Acta A*, 135 (2015), 39.
- [30] BOYD R.W., *Nonlinear Optics*, 2nd ed., Academic Press, New York, 2003.
- [31] VARSANYI G., *Assignments for Vibrational Spectra of Seven Hundred Benzene Derivatives*, Vol. I, Adam Hilger, London, 1974.
- [32] BELLAMY L.J., *The Infrared Spectra of Complex Molecules*, 3rd ed., Wiley, New York, 1975.
- [33] KOGLIN E., WITTE E.G., MEIER R.J., *Vib. Spectros.*, 33 (2003), 49.

Received 2016-07-25

Accepted 2018-08-07